

146, 245 (1982).

4. J. W. Truman, *ibid.* **95**, 281 (1974).

5. A. M. Handler and R. J. Konopka, *Nature* **279**, 236 (1979).

6. J. Ewer, B. Frisch, M. J. Hamblen-Coyle, M. Rosbash, J. C. Hall, *J. Neurosci.* **12**, 3321 (1992).

7. J. M. Giebultowicz, J. G. Riemann, A. K. Raina, R. L. Ridgway, *Science* **245**, 1098 (1989).

8. I. F. Emery, J. M. Noveral, C. F. Jamison, K. K. Siwicki, *Proc. Natl. Acad. Sci. U.S.A.* **94**, 4092 (1997).

9. J. M. Giebultowicz and D. M. Hege, *Nature* **386**, 664 (1997); D. Hege, R. Stanewsky, J. C. Hall, J. M. Giebultowicz, *J. Biol. Rhythms* **12**, 300 (1997).

10. R. J. Konopka and S. Benzer, *Proc. Natl. Acad. Sci. U.S.A.* **68**, 2112 (1971).

11. A. Sehgal, J. L. Price, B. Man, M. W. Young, *Science* **263**, 1603 (1994).

12. A. Sehgal, A. Ousley, M. Hunter-Ensor, *Mol. Cell. Neurosci.* **7**, 165 (1996).

13. R. F. Johnson, R. Y. Moore, L. P. Morin, *Brain Res.* **460**, 297 (1988).

14. S. M. Argamas *et al.*, *Biophys. Chem.* **56**, 3 (1995).

15. J. P. McMillan, H. C. Keatts, M. Menaker, *J. Comp. Physiol.* **102**, 251 (1975).

16. J. W. Truman, *ibid.* **81**, 99 (1972).

17. D. A. Wheeler, M. J. Hamblen-Coyle, M. S. Dushay, J. C. Hall, *J. Biol. Rhythms* **8**, 67 (1993).

18. R. N. Van Gelder, H. Bae, M. J. Palazzolo, M. A. Krasnow, *Curr. Biol.* **5**, 1424 (1995); R. N. Van Gelder and M. A. Krasnow, *EMBO J.* **15**, 1625 (1996).

19. J. C. Hall, *Trends Neurosci.* **18**, 230 (1995).

20. C. Brandes *et al.*, *Neuron* **16**, 687 (1996).

21. J. D. Plautz *et al.*, *J. Biol. Rhythms* **12**, 204 (1997).

22. R. Stanewsky, C. F. Jamison, J. D. Plautz, S. Kay, J. C. Hall, *EMBO J.* **16**, 5006 (1997).

23. *per-luc* transgenics refer specifically to the *pl01a-1* line described in (20). The *per*-promoter-GAL4 fusion gene (*per*-GAL4) was made as has been done with other promoters (37). The construct contains the same 4.2-kb genomic fragment used in the *per-luc* fusion (20) upstream of the GAL4 gene and the *hsp-70* terminator. This fragment was ligated into the P element transformation vector CaspeR4 (38). Six transformants with different insertion sites were generated. The spatial expression patterns of *per*-GAL4 in the adult head in these lines were studied by immunohistochemistry in flies carrying these GAL4 elements and either UAS-*lacZ* or UAS-Tau (39). Three of the six lines express GAL4 in various ectopic tissue locations as well as in a few of the normal *per*-expressing cells [see for example (6, 40)]. The other three lines were relatively normal in their expression patterns and had GAL4-mediated staining in several identified *per* neurons (cf. 6, 40). However, GAL4 expression in these three lines exhibited some differences from the endogenous *per* expression, such as weak eye expression and ectopic expression in the brain's central complex. The line used in this study is one of the latter three. To generate the actual fluorescent flies, we crossed these *per*-GAL4 flies to another transgenic line that drives GFP from the yeast UAS sequence [UAS-GFP (41)].

24. Automated bioluminescent monitoring was carried out as previously described (22), with some modifications. Cultured explants were loaded individually into wells of black microtiter plates previously prepared with 100 μ l of tissue culture medium (see below). Wells were covered with TopSeal with no ventilation hole. Bioluminescence was automatically counted for 15 s about once per hour. Data were analyzed with the Import and Analysis macro set for Microsoft Excel. Primary explants were removed from whole animals that had been entrained to a 12:12 LD cycle. Flies were briefly anesthetized with CO₂ and immediately separated into heads, thoraxes, and abdomens. Further dissections were performed on the individual body parts. Operations were carried out in a tissue culture medium consisting of (by volume) 85.9% S3 insect tissue culture media, 12% fetal bovine serum (heat inactivated for 30 min at 60°C), 1% penicillin-streptomycin mixture, 1% luciferin solution, and 0.1% insulin (1 mg/ml) solution. Cultures were monitored in the same solution throughout the experiment. The concentration of the

luciferin solution varied from experiment to experiment, yielding a final concentration between 0.05 and 0.5 mM. Different concentrations of luciferin did not affect the period or phase of the rhythms, although higher concentrations led to brighter overall bioluminescence.

25. Flies were initially anesthetized with CO₂ followed by a drop of ether. Samples were observed with a long-pass GFP filter cube (Chroma) on an Olympus AX-70 upright microscope; images were collected with a color charge-coupled device camera (Hamamatsu). Images were processed with Adobe Photoshop.

26. J. D. Plautz *et al.*, *Gene* **173**, 83 (1996).

27. R. F. Stocker, *Cell Tissue Res.* **275**, 3 (1994).

28. J. D. Plautz and S. A. Kay, data not shown.

29. P. E. Hardin, *Mol. Cell. Biol.* **14**, 7211 (1994).

30. X. Liu, L. Lorenz, Y. Qiang, J. C. Hall, M. Rosbash, *Genes Dev.* **2**, 228 (1988).

31. D. K. Welsh, D. E. Logothetis, M. Meister, S. M. Reppert, *Neuron* **14**, 697 (1995).

32. J. M. Power, J. M. Ringo, H. B. Dowse, *J. Neurogenet.* **9**, 227 (1995).

33. L. P. O'Keefe and H. D. Baker, *Physiol. Behav.* **41**,

193 (1987).

34. M. Martinez-Gomez, Y. Cruz, M. Salas, R. Hudson, P. Pacheco, *ibid.* **55**, 651 (1994).

35. D. P. King *et al.*, *Cell* **89**, 641 (1997).

36. Z. S. Sun *et al.*, *ibid.* **90**, 1003 (1997); H. Tei *et al.*, *Nature* **389**, 512 (1997).

37. L. Luo, Y. J. Liao, L. Y. Jan, Y. N. Jan, *Genes Dev.* **8**, 1787 (1994).

38. C. S. Thummel, A. M. Boulet, H. D. Lipshitz, *Gene* **74**, 445 (1988).

39. K. Ito, H. Sass, J. Urban, A. Hofbauer, S. Schneuwly, *Cell Tissue Res.* **290**, 1 (1997).

40. K. K. Siwicki, C. Eastman, G. Petersen, M. Rosbash, J. C. Hall, *Neuron* **1**, 141 (1988).

41. Provided by B. J. Dickson.

42. We thank R. Stanewsky and B. J. Dickson for sharing fly lines and P. Hardin, J. Giebultowicz, and K. Siwicki for sharing unpublished data. This work was supported by National Institute of Mental Health grant MH-51573 (to S.A.K. and J.C.H.) and the NSF Center for Biological Timing (to S.A.K.).

19 August 1997; accepted 23 September 1997

The Filamentous Phage pIV Multimer Visualized by Scanning Transmission Electron Microscopy

Nora A. Linderoth, Martha N. Simon, Marjorie Russel*

A family of homomultimeric outer-membrane proteins termed secretins mediates the secretion of large macromolecules such as enzymes and filamentous bacteriophages across bacterial outer membranes to the extracellular milieu. The secretin encoded by filamentous phage f1 was purified. Mass determination of individual molecules by scanning transmission electron microscopy revealed two forms, a unit multimer composed of about 14 subunits and a multimer dimer. The secretin is roughly cylindrical and has an internal diameter of about 80 angstroms, which is large enough to accommodate filamentous phage (diameter of 65 angstroms).

Filamentous phage-encoded pIV is an outer-membrane protein required for phage assembly that is not a part of the virus particle. It has sequence similarity to a family of bacterial proteins that are essential components of the type II and type III protein secretion systems that have been identified in many pathogenic Gram-negative species (1, 2). The members of this protein family (called secretins) are believed to play similar roles in mediating translocation of substrates across the outer membrane. *Gene IV* could be derived from a bacterial gene because some phages contain the gene in different parts of their otherwise colinear genomes and CTX, the lysogenic filamentous phage of *Vibrio cholerae* that encodes cholera toxin (3), lacks it entirely; CTX may use a *V. cholerae* secretin for phage assembly. In addition to a secretin, the type II, type III, and phage assembly systems include a protein containing an essential nucleotide-

binding motif. The remaining components (~13 for type II secretion, ~20 for type III secretion, and 9 encoded by filamentous phage) are related within, but not between, systems.

Bacteria productively infected by filamentous phage remain viable and can continue to grow and divide indefinitely while producing and releasing phage particles. During assembly, the cytoplasmic single-stranded DNA phage genome is extruded through the cytoplasmic membrane where it becomes coated with the phage-encoded capsid proteins that reside in the cytoplasmic membrane before their incorporation into phage (4). Secretion across the outer membrane appears to be concomitant with assembly because periplasmic phage has not been detected. Thus, phage assembly and the type II and III systems all require transport of macromolecules across two bacterial membranes.

The pIV protein exists as a homomultimer that has been previously estimated to consist of 10 to 12 monomers (5). Several of the bacterial homologs form mixed multimers with pIV in vivo, implying structural relatedness and suggesting that they them-

N. A. Linderoth and M. Russel, Rockefeller University, 1230 York Avenue, New York, NY 10021, USA.
M. N. Simon, Department of Biology, Brookhaven National Laboratory, Upton, NY 11973, USA.

*To whom correspondence should be addressed. E-mail: russelm@rockvax.rockefeller.edu

selves also function as multimers. For several homologs, direct evidence of multimer formation is now available (6–8), and one (9) was shown to be a multimer a decade before it was identified as a member of this protein family. The pIV multimer is unusually resistant to dissociation, as are several other secretins (7, 10, 11). Domain swap experiments between pIVs from related phages implicate the NH₂-terminus as a specificity determinant for the choice of filamentous phage to be assembled (12), whereas the NH₂-terminus of a type II homolog is necessary for an interaction with substrates, a finding that can account for the species specificity of secretion (8). The fact that secretins exist as large multimers and that in each assembly-secretion system they appear to be the sole integral outer-membrane component suggests that they may form channels in the outer membrane through which secreted enzymes or assembling structures pass. Of necessity, secretin channels would have to be much larger than previously characterized outer-membrane channels, which allow passage of

small molecules (~600 kD) and have internal diameters of ~11 to 20 Å (13). Filamentous phage is 65 Å in diameter (type IV pili are 55 Å), and several of the folded proteins secreted by type II systems are quite large. Structure-based calculations suggest that 10 to 12 pIV monomers could be arranged to accommodate a sufficiently large pore (14).

Functional His-tagged pIV (monomer molecular weight of 44,619) derived from filamentous phage f1 was solubilized from crude *Escherichia coli* membranes in non-ionic detergent and purified by nickel-chelate and size exclusion chromatography (15, 16). More than 90% of the pIV eluted at or above ~600 kD, which is consistent with previous results indicating that all pIV extracted from cells is multimeric. The purity of pIV, estimated by comparison of immunoblots and stained samples from acrylamide and agarose gels, was ≥95%.

pIV was imaged in the scanning transmission electron microscope (STEM). The STEM is unique in its ability to visualize individual biological molecules directly

without staining, fixing, or shadowing. The microscope operates in a dark-field mode, and high-efficiency annular detectors collect nearly all the scattered electrons. The number of electrons scattered is directly proportional to the mass thickness at that point, so that molecular weights of individual objects (or portions of them) can be calculated. The images are recorded digitally, in focus, and as such are directly interpretable. A typical image is shown in Fig. 1. Aside from the tobacco mosaic virus (TMV), which was added as a standard, several species are distinguishable: Rectangular objects and pairs of rectangles predominate, and some rings are also present. The double rectangles and rare brighter rings have similar masses, ~1240 kD (Table 1), suggesting that they represent two views of the same object. The single rectangles and less intense rings have masses of ~615 kD, which suggests that there are about 14 pIV monomers per multimer. This finding is consistent with previous estimates of the pIV multimer on the basis of its *S* value and elution from sizing columns (5, 15). The 1240-kD structures are presumably dimers of multimers, which may reflect formation of head-to-head or tail-to-tail complexes; indirect evidence suggests that dimer formation occurs during purification (15).

Specimens stained with methylamine vanadate and examined in the STEM provide more detail (Fig. 2). The most abundant structure is roughly rectangular and has dimensions similar to those of the rectangle pairs seen in the unstained preparations. It consists of two long curved rods connected by two straight crosspieces and probably connected at the ends as well. Single units of this “ladder-like” structure are presumably the 615-kD species. The single rectangles (Fig. 3B) look remarkably like cartoons of the pIV multimer drawn to

Fig. 1. Dark-field STEM images of unstained pIV. A 3- μ l sample of pIV in 1% CHAPS, 25 mM Hepes (pH 8.0), 0.5 M NaCl, 0.5 mM EDTA, and 0.5 mM benzamidine was injected into a drop of buffer on a thin carbon film (2 to 3 nm) supported by a holey thick carbon film on a titanium grid to which TMV had been previously applied as an internal mass calibration standard (21). The grid was washed five times with 5 μ l of 100 mM ammonium acetate and 10 times with 5 μ l of 20 mM ammonium acetate, quick frozen in a liquid nitrogen slush, and dried under vacuum. The STEM images were made with the Brookhaven Biotechnology Resource instrument (21). The full scale of the portion of the micrograph shown is 325 nm by 390 nm and the bar indicates 200 Å. The double-headed arrow indicates double rectangles, arrows indicate single rectangles, and arrowheads indicate rings.

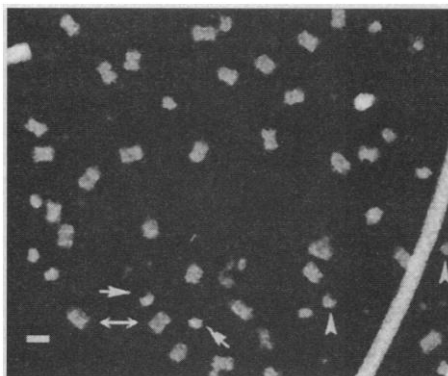
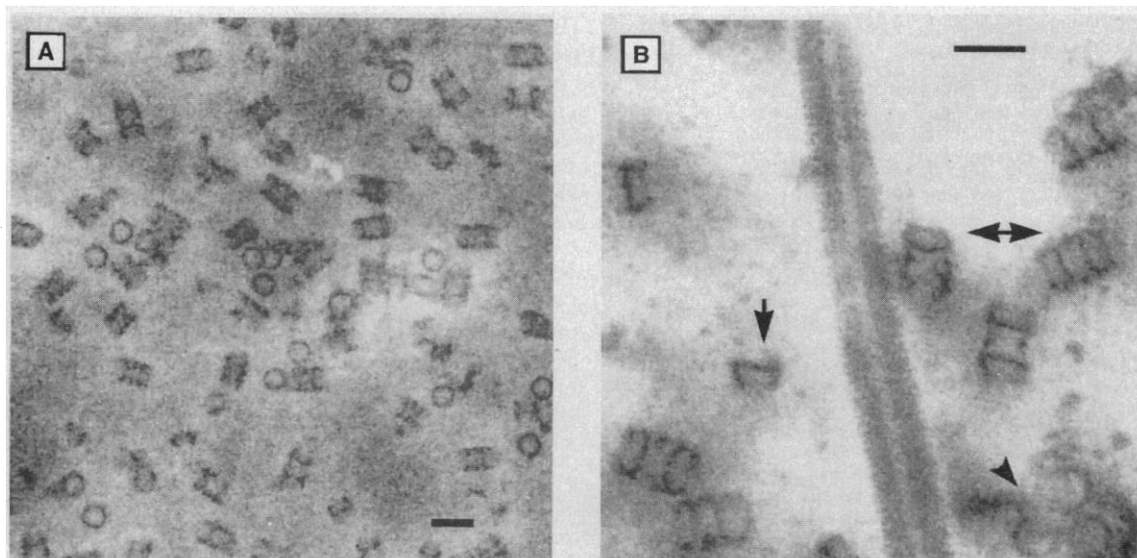


Fig. 2. Methylamine vanadate-stained STEM images of pIV. A sample of pIV was applied to a grid to which TMV had already been added and washed as described in Fig. 1, except that the final wash was with 2% methylamine vanadate and the grid was air dried. Full scale of the micrograph is 512 nm in (A) and 128 nm in (B); the bars indicate 200 Å. The arrows are as in Fig. 1.



interpret its physical properties (2, 8, 17). The ringlike species is also present; examples in Fig. 3C illustrate the large central cavity, which was not apparent in the lower resolution unstained images.

An extract from cells that lacked pIV was subjected to the same two-column purification procedure used to isolate pIV, and the corresponding sample was examined in the STEM. The control preparation had one-tenth the amount of protein, and even concentrated samples lacked structures with the mass and appearance of those seen in the authentic preparation (18). A sample of pIV was incubated with polyclonal rabbit antibody to pIV, reisolated on a size exclusion column to remove unbound antibody, and examined in the STEM. The images were complex because of cross-linking by the antibody, and only isolated rectangles were used for mass measurements. Their average mass was substantially larger than the value determined for rectangles in the absence of antibody (1580 ± 190 versus 1250 ± 40 for dimers and 790 ± 40 versus 610 ± 20 for monomers); the greater standard deviation of measurements for pIV plus antiserum is presumably due to variable numbers of antibody molecules bound per pIV multimer. Taken together, these controls provide strong evidence that the structures detected in the STEM are pIV multimers.

The dimensions of the methylamine vanadate-stained structures were quite regular (Table 1). With the added TMV (diameter of 180 Å) as a reference standard, the ring form has an external diameter of ~140 Å and an internal diameter of ~80 Å. The external diameter of the ladder along the crosspieces is ~130 Å (internal diameter of ~80 Å). These values also suggest that the two forms are different views of the same object. They indi-

cate that pIV is cylindrical and has an internal hole sufficient to accommodate filamentous phage. As measured in the STEM with TMV as a standard, filamentous phage was 66 to 68 Å in diameter (18).

The contour length of the double rectangle is ~210 Å, whereas that of the single is ~70 Å. The single rectangles have curved ends and a single crosspiece with the same dimensions as the larger structure, but the portion of the larger structure that lies between the two crosspieces is rarely visible in the single rectangle (compare Fig. 3, A and B); hence, the average length of single rectangles is less than half that of the double. Perhaps the hidden ends of this segment are hydrophobic and either bury themselves within a single multimer or self-associate to form dimers of multimers. This phenomenon may be related to the oriented rosettes that form when detergent is removed from puri-

fied influenza hemagglutinin and neuraminidase, leaving the hydrophobic domains at the core (19). This, in turn, would suggest that the "sticky" end is the COOH-terminal portion of the protein, which is normally embedded in the outer membrane, and thus that the curved arms constitute the periplasmic domain that confers specificity to the secretion-assembly process and potentially gates the channel. A single ~70 Å-long multimer could span the outer membrane, which is ~25 Å thick (20), and still have a substantial periplasmic domain. The crosspiece itself, which encircles the central channel, could serve as a reinforcing ring that provides the resistance to dissociation that appears to be characteristic of most secretins.

REFERENCES AND NOTES

1. M. Hobbs and J. S. Mattick, *Mol. Microbiol.* **10**, 233 (1993); A. P. Pugsley, *Microbiol. Rev.* **57**, 50 (1993); G. Salmond and P. Reeves, *Trends Biochem. Sci.* **18**, 7 (1993); S. Genin and C. A. Boucher, *Mol. Gen. Genet.* **243**, 112 (1994); C. A. Lee, *Trends Microbiol.* **5**, 148 (1997).
2. M. Russel, *Science* **265**, 612 (1994).
3. M. K. Waldor and J. J. Mekalanos, *ibid.* **272**, 1910 (1996).
4. P. Model and M. Russel, *Bacteriophages* **2**, 375 (1988); M. Russel, *Mol. Microbiol.* **5**, 1607 (1991); H. Endemann and P. Model, *J. Mol. Biol.* **250**, 496 (1995); M. Russel, *Trends Microbiol.* **3**, 223 (1995).
5. B. I. Kazmierczak, D. L. Mielke, M. Russel, P. Model, *J. Mol. Biol.* **238**, 187 (1994).
6. L.-Y. Chen, D.-Y. Chen, J. Miaw, N.-T. Hu, *J. Biol. Chem.* **271**, 2703 (1996).
7. K. R. Hardie, S. Lory, A. P. Pugsley, *EMBO J.* **15**, 978 (1996).
8. V. E. Shevchik, J. Robert-Badouy, G. Condemine, *ibid.* **16**, 3007 (1997).
9. W. J. Newhalp, C. E. Wilde III, W. D. Sawyer, R. A. Haak, *Infect. Immun.* **27**, 475 (1980).
10. S. L. Drake and M. Koomey, *Mol. Microbiol.* **18**, 975 (1995).
11. N. A. Linderth, P. Model, M. Russel, *J. Bacteriol.* **178**, 1962 (1996).
12. S. Daefler, M. Russel, P. Model, *J. Mol. Biol.* **266**, 978 (1997).
13. J. Liu, J. M. Rutz, J. B. Feix, P. E. Klebba, *Proc. Natl. Acad. Sci. U.S.A.* **90**, 10653 (1993); H. Nikaido, *J. Biol. Chem.* **269**, 3905 (1994).
14. M. Russel, N. A. Linderth, A. Sali, *Gene* **192**, 23 (1997).
15. N. A. Linderth, M. Russel, P. Model, unpublished results.
16. In brief, His-tagged pIV, with His(x7) inserted after Ala³⁰⁸ and Ser³¹⁸ → Ile (17) was expressed from plasmid pPMR132. Cells were lysed after incubation with lysozyme and treated with ribonuclease A and deoxyribonuclease I, and the membranes were isolated by centrifugation and suspended in buffer containing the nonionic detergent octyl-poly-oxyethylene (4%). Solubilized material was bound to Ni-Sepharose beads, washed with buffer containing 1% CHAPS, and eluted with imidazole in the same buffer. The pIV-containing fractions were pooled, concentrated, and chromatographed on Bio-Gel A5M (Bio-Rad, Hercules, CA), also in buffer containing 1% CHAPS. Peak fractions were used for the STEM.
17. M. Lindeberg, G. P. C. Salmond, A. Collmer, *Mol. Microbiol.* **20**, 175 (1996).
18. N. A. Linderth, M. N. Simon, M. Russel, data not shown.
19. W. G. Laver and R. C. Valentine, *Virology* **38**, 105 (1969).
20. W. Cowan *et al.*, *Nature* **358**, 727 (1992); T. Schirmer, T. A. Keller, Y.-F. Wang, J. P. Rosen-

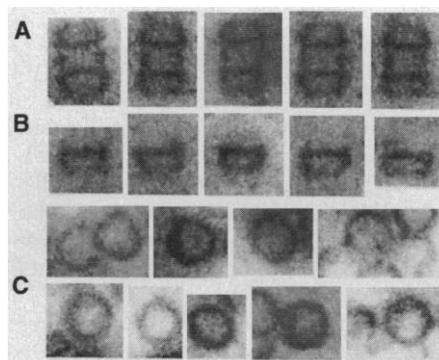


Fig. 3. Montage of pIV species from bright-field STEM images of methylamine vanadate-stained specimens as described in Fig. 2. (A) 1240-kD species; (B) 615-kD species; and (C) top or ring views.

Table 1. Dimensions and mass of pIV. Digital images were recorded from the bright-field detector (for stained samples) or the annular dark-field detector (for unstained samples). The dimensions of both TMV and specimen particles in methylamine vanadate-stained samples (Fig. 2) were measured with the program NIH Image and converted to angstroms with the diameter of TMV (180 Å) as a standard. For mass measurements, unstained samples were used. Areas with clean background and adequate numbers of both TMV and specimen particles (Fig. 1) were selected. The background was computed for clear areas and subtracted from the intensity summed over each particle. The STEM calibration factor was checked in each image against that of TMV; the summed intensities (minus the background) multiplied by this calibration factor give mass values for the specimens. ND, not determined.

	Stained		Unstained		Mass (kD)
	Number counted	Outer dimension (Å)	Inner dimension (Å)	Number counted	
Double ring	ND	ND	ND	17*	1230 ± 50
Single ring	23	140 ± 10	80 ± 10	44†	620 ± 40
Double rectangle				152	1250 ± 40
Length	31	210 ± 10			
Width	33	130 ± 10	80 ± 10		
Single rectangle				47	610 ± 20
Length	17	70 ± 10			
Width	9	140 ± 10	70 ± 10		

*Bright images. †Less bright images.

busch, *Science* **267**, 512 (1995).

21. J. S. Wall, in *Introduction to Analytical Electron Microscopy*, J. J. Hren, J. I. Goldstein, D. C. Joy, Eds. (Plenum, New York, 1979), pp. 333-342; J. S. Wall, J. F. Hainfeld, K. D. Chung, in *Proceedings of the 43rd Annual Meeting of the Electron Microscopy Society of America*, G. W. Bailey, Ed. (San Francisco

Press, San Francisco, CA, 1985), pp. 716-717; J. S. Wall and J. F. Hainfeld, *Annu. Rev. Biophys. Chem.* **15**, 355 (1986).

22. We thank P. Model for suggestions, interest, encouragement, and criticism of the manuscript; B. Lin for STEM specimen preparation; and J. Wall for helpful discussions about the data analysis. Supported by

NSF grant MCB93-16625 (M.R.). The Brookhaven National Laboratory STEM is an NIH Supported Resource Center (NIH grant P41-RR01777), with additional support provided by the U.S. Department of Energy, Office of Health and Environmental Research.

15 August 1997; accepted 21 October 1997

Nuclear Accumulation of NFAT4 Opposed by the JNK Signal Transduction Pathway

Chi-Wing Chow, Mercedes Rincón, Julie Cavanagh, Martin Dickens, Roger J. Davis*

The nuclear factor of activated T cells (NFAT) group of transcription factors is retained in the cytoplasm of quiescent cells. NFAT activation is mediated in part by induced nuclear import. This process requires calcium-dependent dephosphorylation of NFAT caused by the phosphatase calcineurin. The c-Jun amino-terminal kinase (JNK) phosphorylates NFAT4 on two sites. Mutational removal of the JNK phosphorylation sites caused constitutive nuclear localization of NFAT4. In contrast, JNK activation in calcineurin-stimulated cells caused nuclear exclusion of NFAT4. These findings show that the nuclear accumulation of NFAT4 promoted by calcineurin is opposed by the JNK signal transduction pathway.

JNK is a member of the mitogen-activated protein (MAP) kinase group that is activated in response to cytokines and exposure to environmental stress (1). Substrates of the JNK protein kinase include the transcription factors ATF2, Elk-1, and c-Jun (2). JNK phosphorylates each of these transcrip-

tion factors within the activation domain and increases transcriptional activity (2). Genetic studies of JNK indicate that this signaling pathway involves multiple cellular processes (3). Here, we show that one of these processes is the regulated nuclear accumulation of NFAT4.

Substrate recognition by JNK requires the interaction of the kinase with a region of the substrate that is distinct from the sites that are phosphorylated (2). We used this specific binding interaction to identify JNK substrates with the two-hybrid method (4). Fourteen independent cDNA clones that encode the transcription factor

NFAT4 were obtained from an embryonic cDNA library. NFAT4 (also known as NFATx and NFATC3) is a member of the REL domain family of transcription factors that are important mediators of immune responses (5, 6). In contrast to the other members of the NFAT group, which are primarily expressed in peripheral T cells (NFATc and NFATp), the NFAT4 isoform is expressed in immature thymocytes and nonlymphoid tissues (5-7). Because JNK is implicated in both innate (3, 8) and acquired (9) immune responses, the interaction between JNK and NFAT4 may be biologically important.

To test whether JNK and NFAT4 interact in mammalian cells, we performed co-immunoprecipitation assays using extracts prepared from transfected cells. Immunoblot analysis demonstrated the presence of JNK in NFAT4 immunoprecipitates (Fig. 1A). Control experiments showed that JNK was not detected in NFAT3 immunoprecipitates (Fig. 1A). These data indicate that JNK interacts with NFAT4 in vivo. To confirm that JNK binds directly to NFAT4, we performed in vitro binding assays with recombinant proteins. JNK2 bound strongly to NFAT4 but not to NFAT3 (Fig. 1B). Similar data were obtained in experiments using JNK1 (10). The amount of JNK binding to NFAT4 was approximately five times the amount of binding to c-Jun (10). Deletion analysis demonstrated that the mini-

C.-W. Chow, J. Cavanagh, M. Dickens, R. J. Davis, Howard Hughes Medical Institute, Program in Molecular Medicine, Department of Biochemistry and Molecular Biology, University of Massachusetts Medical School, Worcester, MA 01605, USA.

M. Rincón, Program in Immunobiology, Department of Medicine, University of Vermont, Burlington, VT 05405, USA.

*To whom correspondence should be addressed.

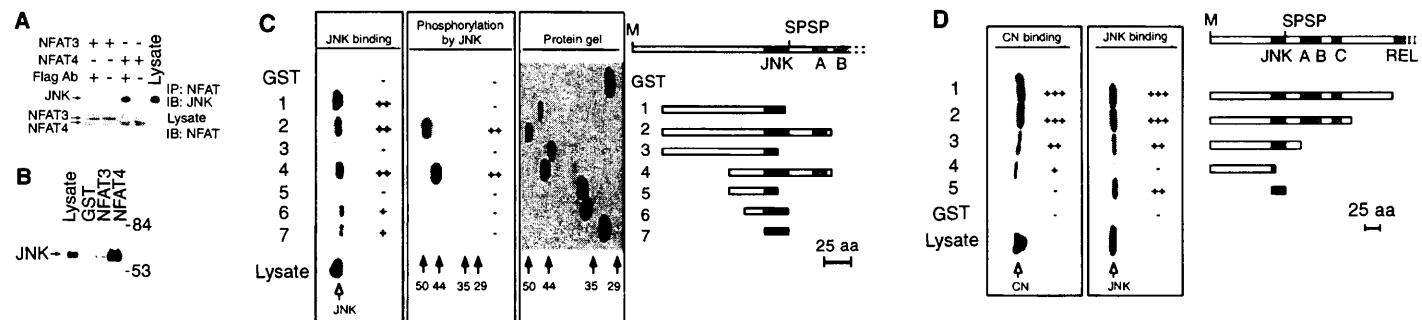


Fig. 1. Interaction of NFAT4 with the JNK protein kinase. **(A)** NFAT4 and JNK interact in vivo. Epitope-tagged HA-JNK2, Flag-NFAT3, and Flag-NFAT4 were expressed in COS cells. NFAT3 and NFAT4 were immunoprecipitated with mAb M2. HA-JNK2 in the immunoprecipitates (IP) was detected by protein immunoblot (IB) analysis with mAb 12CA5 (Boehringer-Mannheim). The NFAT3 and NFAT4 proteins in the cell lysates were detected by protein immunoblot analysis. **(B)** Binding of JNK to the NH₂-terminal region of NFAT4. NFAT4(1-207) and NFAT3(1-218) were fused to GST. The purified recombinant NFAT proteins were used to bind epitope-tagged HA-JNK2 (17). Bound JNK2 was detected by protein immunoblot analysis. Molecular size markers are indicated (in kilodaltons). **(C)** Identification of the

JNK binding site. The NFAT4 proteins correspond to NFAT4 residues 35 to 154, 32 to 207, 32 to 146, 93 to 207, 93 to 146, 113 to 162, and 136 to 162 fused to GST. The purified recombinant NFAT4 proteins were examined by SDS-PAGE (Coomassie staining), as substrates for JNK2 (17), and in binding assays with JNK2 (17). The phosphorylation of NFAT4 was detected after SDS-PAGE by autoradiography. Bound JNK2 was detected by protein immunoblot analysis. **(D)** Binding of JNK and calcineurin to different sites on NFAT4. The NFAT4 proteins correspond to NFAT4 residues 1 to 413, 1 to 333, 1 to 207, 1 to 146, and 136 to 162 fused to GST. The immobilized NFAT proteins were incubated with cell extracts. Bound JNK2 and calcineurin were detected by protein immunoblot analysis.